2-D CFD Computations of the Two-Bladed Darrieus-Type Wind Turbine

K. Rogowski[1†], M. O. L. Hansen[2] and P. Lichota[1]

[1] *Institute of Theoretical and Applied Mechanics, Warsaw University of Technology, Warsaw, 00-665, Poland*
[2] *DTU Wind Energy, Technical University of Denmark, Lyngby, 2800 Kgs., Denmark*

†*Corresponding Author Email: krogowski@meil.pw.edu.pl*

ABSTRACT

In spite of the attractiveness of CFD methods and advanced measurement methods, there is still no full analysis of aerodynamic blade loads for vertical axis Darrieus-type wind turbines. Due to an inherently unsteady flow around the rotor blades, blade-wake-blade interaction and the occurrence of dynamic stall, the aerodynamics of this type of wind turbine is very complex. A two-bladed rotor have been investigated numerically for the tip speed ratio of 5.0. This paper compares results for aerodynamic blade loads obtained applying such turbulence models as: the standard k-ε; the RNG k-ε; the Realizable k-ε and the SST k-ω. As a result, quantitative instantaneous blade forces as well as instantaneous wake profiles behind the rotor have been obtained. Aerodynamic wake behind the rotor is also visualized by using streak lines. All CFD results are compared with experimental data taken from literature. Good agreement between the numerical results and the experiment is shown for the aerodynamic blade loads as well as for aerodynamic wake behind the rotor.

Keywords: Wind turbine; Aerodynamic blade loads; Aerodynamic wake; Streak line.

NOMENCLATURE

b	blade displacement	V_W	water velocity at the rotor
c	blade chord length	V_x	streamwise perturbation velocity
C_N	normal force coefficient	V_y	lateral perturbation velocity
C_T	tangential force coefficient	W	relative velocity
Cp	power coefficient	**Greek letters**	
F_N	normal aerodynamic blade load	α	angle of attack
F_T	tangential aerodynamic blade load	γ	pitch angle
N	number of blades	θ	azimuth position of the rotor
R	rotor radius	σ	solidity
TSR	tip speed ratio	ω	angular velocity of the rotor
u	dimensionless streamwise velocity	V	water velocity
v	dimensionless lateral velocity		

1. INTRODUCTION

The aerodynamic efficiency of a wind turbine is expressed as a power coefficient *Cp* versus dimensionless tip speed ratio (*TSR*). A typical curve of the power coefficient for the Darrieus wind turbine is presented in Fig. 1 according to Paraschivoiu (2002). The characteristic of the power coefficient is divided into three regions depending on the physical phenomena occurring in the rotor area. In the first section of the curve (part A), corresponding to low tip speed ratios (approximately below *TSR* of 4), the dynamic stall effects are important because of large variations and high angles of attack. These effects are associated with large scale vorticity shed from the airfoil and convected in the wake. The dynamic effects (also known as the primary effects) depend on a solidity σ=cN/R, where c is the chord, N is the number of blades, and *R* is the rotor radius. In the third section of the *Cp* curve (part C), for the high tip speed ratios, the secondary effects such as a rotating shaft, struts, airfoil shape, spoilers etc. are important. In the range of tip speed ratio between 4 and 6 (part B), a wind turbine has its optimal aerodynamic efficiency (maximum power coefficient) and the

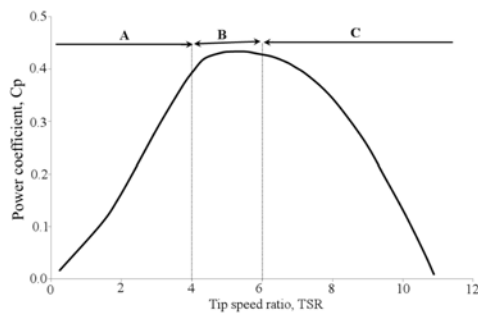contribution of all the effects is visible.

Fig. 1. Typical characteristics of the power coefficient.

Since the 70s, many aerodynamic methods for the Darrieus turbine have been developed. The most popular methods are streamtube models, vortex models and computational fluid dynamics (CFD). The models differ each other in level of complexity and level of accuracy. The most common aerodynamic methods based on Glauert's concept are known as streamtube models. They enable to predict aerodynamic performance of the rotor in a short time and do not require excessive computing resources. This approach is often sufficient from an engineering point of view. The momentum-based methods, however, fail above the solidity of 0.2. Furthermore, they are inadequate for wind farm applications because of their deficiencies in the calculation of near-wake structure see Shen *et al.* (2009). Another class of aerodynamic methods used for the Darrieus wind turbines is vortex wake methods. These methods are more complicated and usually they are used for more detailed and more accurate computations. Vortex methods can be divided into two types: prescribed wake models and free wake models. The first type of methods is faster while the second one gives more physical results (Shen *et al.* (2009)). Vortex methods and momentum methods can be combined with other methods. Moreover, they are not deterministic, but require imported airfoil data from outside, e.g. from wind tunnel experiments or computed airfoil data. Furthermore, they require dynamic stall models. Alternatively, there are the Navier-Stokes equations based methods that are much more time-consuming as opposed to the previously mentioned methods Rogowski *et al.* (2017). Noticed the above methods do not cover all the possibilities for the Darrieus concept (Shamsoddin and Porté-Agel 2014; Ponta and Jacovkis, 2001).

Despite huge progress in computational methods of fluid dynamics, there are only few numerical studies for aerodynamic blade loads of the Darrieus wind turbine comparing with experiments. The biggest problem is the lack of experimental data for aerodynamic forces especially for three-dimensional rotors. Since the 70s only Strickland *et al.* (1981) and Oler *et al.* (1983) have tried to measure the aerodynamic blade forces for the case corresponding to the two-dimensional vertical axis wind turbine (VAWT). Airfoil characteristics, lift and drag coefficients as a function of the angle of attack, for rotating blades of a VAWT were

investigated by Laneville and Vittecoq (1986) in the wind tunnel. The aerodynamic behavior of oscillating NACA 0018 airfoil under the dynamic stall conditions was researched by Wickens (1985) in a wind tunnel. Recently, the particle image velocimetry (PIV) technique has become popular Simão Ferreira *et al.* (2007). Some authors have shown, that it is possible, though crudely, that blade loading can be extracted from velocity flow using a method that they have developed Simão Ferreira *et al.* (2011).

A scientific review of CFD analysis of aerodynamic blade loads showed that researchers are mainly focusing on dynamic stall effects and heavily loaded rotors. The aspect of dynamic stall was undertaken, for example, by Allet *et al.* (1999). Authors examined unsteady flow over the pitching airfoil NACA 0015 in "Darrieus motion" using the Cebeci-Smith and the Johnson-King turbulence models. Presented by these authors results of aerodynamic forces were investigated for one bladed rotor at a tip speed ratio of 2.5 and at a blade Reynolds number of 67,000. Final results were compared with the experiment of Oler *et al.* (1983). Characteristics of the normal and tangential blade force coefficients suggested that the normal force component covered quite reasonably the experimental results of Oler *et al.* (1983). While, the tangential forces computed using the turbulence models were overestimated in relation to the experiment. CFD investigations of the 2D VAWT based on the Oler experiment was conducted also by Hansen and Sørensen (2001) using the standard k-ε and the Cubic k-ε turbulence models. The obtained results for the normal and tangential force coefficients look reasonable. Another, more extensive work of a similar nature is showed by Simão Ferreira *et al.* (2007). Contrary to presented attempts, this work is focused more on flow aspects under dynamic stall regime (tip speed ratio of 2) than on aerodynamic blade forces. The authors examined the Spalart-Allmaras and the k-ε turbulence models as well as Large Eddy Simulation (LES) and Detached Eddy Simulation (DES) approaches. The obtained results of vorticity in the rotor area were validated based on the Particle Image Velocimetry (PIV) experiment. The numerical investigations seem to confirm the ability of CFD methods to compute the velocity field for the rotor working in the stall regime. Numerical investigations of the NACA 0018 airfoil characteristics for the rotating blades of VAWT and for tip speed ratios of 2 and 7 were performed by Amet *et al.* (2009) based on the experimental results of Laneville and Vittecoq (1986). These computations were made for unsteady compressible RANS equations and the k-ω turbulence model. The authors showed differences between experimental and numerical results of the airfoil characteristics, but the trends for the experimental and numerical curves were similar.

The sliding mesh technique is commonly used for analysis of unsteady flow around the Darrieus-type vertical-axis wind turbine. Wang *et al.* (2014) simulated the influence of interaction between

vortices and rotor blades on the turbine performance employing the Spalart-Allmaras turbulence model. Bianchini *et al.* (2015) confirmed the presence of a virtual incidence on the rotor blades having various airfoils and rotor configurations. These authors investigated a one-bladed rotor employing unsteady Navier-Stockes solver. Numerical study of a single bladed vertical axis wind turbine operating under dynamic stall conditions were performed by Banga *et al.* (2017). These authors investigated a rotor with radius of 1.2m employing the SST k-ω turbulence model and the sliding mesh technique in their research. A small two-bladed vertical-axis wind turbine operating at a moderate tip speed ratio was examined by Rezaeiha *et al.* (2017). Researchers focused on the effect of the domain size on the performance of the two-dimensional rotor. Two-dimensional numerical computations of the flow around a three-straight-bladed Darrieus-type water turbine were performed by Velasco *et al.* (2017) employing the time-accurate Reynolds-averaged Navier-Stokes with the SST k-ω turbulence model. The purpose of the authors was to investigate synthetic jet actuators on a water turbine. Darrieus wind turbine performance with cambered blades for different turbine solidity factor was analyzed by Qamar and Janajreh (2017). The authors analyzed torque and power of two-dimensional turbine as a function of tip sped ratio for various number of blades and chord lengths utilized sliding mesh with k-ω turbulence model.

2. RESEARCH OBJECTIVES

Although the first CFD computations of vertical-axis wind turbine by Rajagopalan and Fanucci (1985) were performed over 30 years ago, it is still grueling how to perform full two-dimensional analysis of the Darrieus wind turbine.

A literature review show that many researchers, focusing on CFD modeling of Darrieus wind turbines, concentrate on rotor performance employing the SST k-ω turbulence model. Moreover, they investigate the influence of the numerical domain, grid distribution, rotor solidity and dynamic stall. A very important issue in CFD modeling of flow around the Darrieus wind turbine is the choice of an appropriate turbulence approach. Therefore, the authors of this paper paid particular attention to examine the SST k-ω model and k-ε family turbulence models.

Small amount of experimental data indicates that conducting such research is difficult and expensive. CFD computations can be helpful in mechanical and structural design of vertical-axis wind turbines. They also can be used in design of experiments. This paper gives guidelines for experimentations who assemble the rotor blades.

From the point of view of the design of wind farms, an aerodynamic wake downstream behind the rotor is a very important issue. Many researchers investigated aerodynamic wake for turbines operating under dynamic stall conditions. This paper extend the state of knowledge of aerodynamic

wake of turbines operating under moderate tip speed ratio.

The purposes of the work are as follows:

1. The assessment of the major turbulence models for the Darrieus-type wind turbine.

2. Examination of aerodynamic forces using CFD methods and compare to the experiments of Strickland *et al.* (1981).

3. Quantitative and qualitative comparison of the wake behind the rotor between CFD approach and the experiment, Strickland *et al.* (1981).

3. AERODYNAMIC LOADS AND AERO-DYNAMIC WAKE

Aerodynamic loads are given as the normal blade load (normal to the swept surface) F_N and the tangential blade load (tangential to the swept surface) F_T (see Fig. 2). These aerodynamic load components depend on: airfoil shape, chord length and Reynolds number. The tangential blade load F_T integrated over the blade trajectory and multiplied by the number of blades determines the torque of the Darrieus rotor. The normal and tangential aerodynamic loads are given through the normal and tangential force coefficients, C_N and C_T, respectively:

$$F_N = 1/2\, C_N \rho A V^2 \qquad (1)$$

$$F_T = 1/2 C_T \rho A V^2 \qquad (2)$$

In Fig. 2 the following variables are introduced: V – water velocity; R – rotor radius; ω – angular velocity of the rotor; ωR – tangential velocity of the rotor blade; V_W – fluid velocity at the rotor; W – relative velocity; α – angle of attack; rotor swept area – A and θ – azimuth position. Both the normal and the tangential forces change with azimuth position. For all graphs of aerodynamic loads presented in the paper, the azimuth of 0° and direction of change of the azimuth is the same as in Figs. 2 and 3.
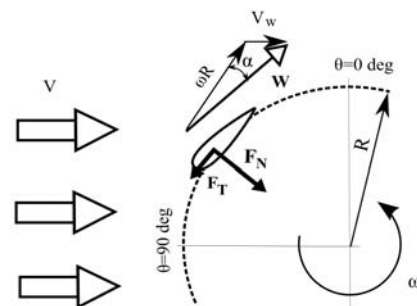

Fig. 2. Aerodynamic blade forces.

A correct computation of wake behind the vertical axis wind turbine is a very important factor from the viewpoint of layout of wind farm. In this article, the structure of the wake behind VAWT is presented by velocity profiles behind the rotor. Figure 3 presents the sampling points of velocity at the distance of

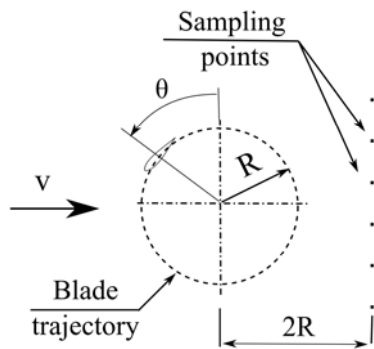one diameter downstream from the rotor axis of rotation.

Fig. 3. Sampling points for velocity profiles.

4. THE EXPERIMENT OF STRICKLAND

Originally, the experiments conducted by Strickland were made in order to confirm abilities of a vortex based model to compute the aerodynamic forces as well as the near-wake structure (Strickland *et al.* 1979a,b; Strickland *et al.* 1981). During the experiments different tests were carried out for three configurations of the rotor. The rotors had one, two or three straight blades using the NACA 0012 airfoil. The radius of the rotor R was 0.61m and the chord c of the airfoil was chosen to be 9.14 cm giving solidity values σ of 0.15, 0.30 and 0.45 for the one-, two- and three-bladed rotor, respectively. Rotor blades were operated in a water tow tank with a tangential velocity of 45.7 cm/s that corresponded to a blade Reynolds number of 40,000. The length of the water tank was 10 meters, the width was 5 meters and the depth was 1.25 meters. The advantage of using water instead of air was easier flow visualization around the rotor, easier to measure blade loads because of lower inertial forces of blades and lower rotational speed for the same Reynolds number.

The rotor was mounted on a special carriage which could slide along a fixed rail. A roller chain system ensured a constant angular velocity of the rotor and the appropriate towing speed. Velocities of towing were 18.3 cm/s, 9.1 cm/s and 6.1 cm/s corresponding to three tip speed ratios of 2.5, 5.0 and 7.5, respectively. Length of blades was chosen to yield conditions corresponding to the two-dimensional flow. The blades were assembled in a specific way. One end of each blade was mounted above the water table to the moving carriage whereas the second end was free. The clearance between free ends of the blades and the bottom of tank was 15 cm. In the experiment of Strickland *et al.* (1981), the velocity field was examined quantitatively by measuring the velocity profiles in the wake behind the rotor.

5. CFD MODEL

All CFD results presented in this paper are obtained using ANSYS Fluent 15.0.

5.1 Turbulence Models

Since the 1940's, two-equations turbulence models have become the basis for modeling turbulent flow. The most popular two-equation models, the k-ε and the k-ω models, are based on two independent scales obtained from two transport equations such as the equation for the turbulence kinetic energy and the equation for its dissipation. Many variants of turbulence models show the difficulty in modeling turbulence. This paper compares results for aerodynamic loads and for wake profiles obtained applying such turbulence models as: the standard k-ε; the RNG k-ε; the Realizable k-ε; and the SST k-ω. All of these models are classical models and are found in most commercial CFD codes and e.g. described in the Theory Guide of ANSYS Fluent Documentation (ANSYS, Version: 15.0.0).

5.2 Geometrical Model

Fig. 4 presents the two-dimensional model of a vertical axis wind turbine used during CFD investigations. This model is placed into a square domain. Basic geometrical parameters such as chord c and rotor radius R are the same as in the experiments of Strickland *et al* (1979a). Fig. 4 shows also the length of the large square domain a. During CFD simulations, the rotor embedded into the circular domain as well as the circular domain rotates relative to the motionless square computational domain. In previous investigations of the corresponding author (Rogowski (2014)), the impact of the length of the square domain on the numerical solution was analyzed. CFD computations confirmed that too small size from the inlet to the rotor results in overestimated results of the rotor power coefficient. Similarly, in the case of the distance from the wind turbine to the side edges of the computational domain. Qamar and Janajreh (2017) examined aerodynamic wake downstream behind a wind turbine using the computational domain size of *10 R* from the rotor axis of rotation, where R is the rotor radius. Rogowski (2014) proved that the minimum length of the square domain should be at least 10 times larger compared to the diameter of the rotor. In this investigation, the authors of the paper assumed that the length of the square domain is 15 meters.
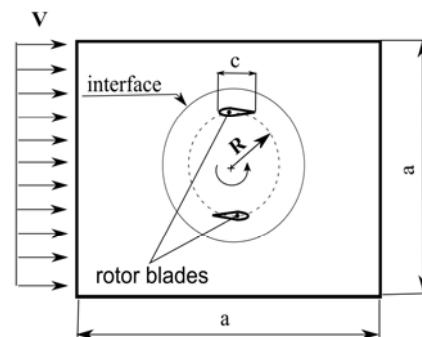

Fig. 4. Geometrical model for CFD simulations.

5.3 Mesh

During 2D unsteady Reynolds averaged Navier–Stokes (URANS) simulations the sliding mesh model

has been used in all presented test cases. Therefore, both the circular and the square domains have been meshed independently. All the CFD results have been obtained using a hybrid mesh consisting of structured quadrilateral elements near airfoils aligned with the boundary layer and unstructured mesh consisting of triangular elements elsewhere. The sliding mesh concept allows adjacent computational domains to slide relative to one another. Moreover, a grid interface provides transfer of data between these two computational domains, ANSYS, Version: 15.0.0 or Ferziger and Perić (2002).

The most important parameters of the mesh that have an influence on the numerical solution are: the length of the square domain, the edge sizing of profiles, the number of layers of structured mesh, the growth rate of structured mesh, the growth rate of unstructured mesh, and the first layer thickness in a direction normal to the wall (wall y+).

The number of divisions of the square domain edges is 30 whereas the number of divisions of the circular domain edge is 200. Fig. 5 presents the mesh of the entire computational domain; the mesh near the edge of the rotating domain; distribution of the mesh around the profile and the mesh near the leading edge of the profile.
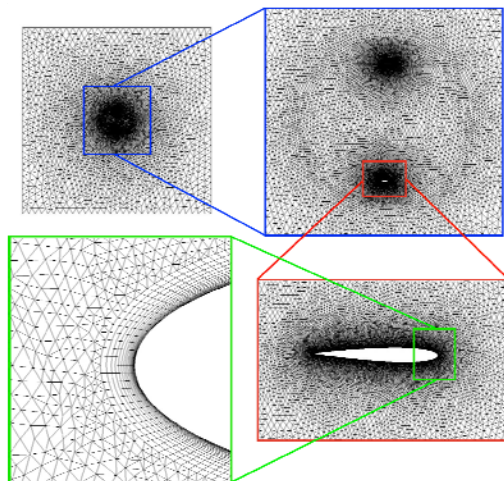

Fig. 5. Mesh distribution for CFD simulation.

In this paper, numerical solution sensitivity test has been performed for the two-bladed rotor working at a tip speed ratio of 5. A mesh-sensitivity study has been performed using the k-ω SST turbulence model and turbulence intensity of 0.1%. Mesh sensitivity test has been performed for the following mesh parameters: the edge sizing of airfoils; the number of layers of structured mesh; the growth rate of structured mesh and the global growth of unstructured mesh. The criterion of the wall y+~1 has been met for all test cases.

Research has showed that the structured mesh growth rate and its layers number are important factors. Fig. 6 presents the results of the tangential force as a function of the azimuth position for three values of structured mesh growth rate (GRI). These values are: 1.2; 1.3 and 1.4, Mesh 1, Mesh 2 and Mesh 3, respectively. As it can be seen from the graph, mesh layers growth near the walls of the

profile should be 1.2. Studies have shown that the number of layers should be minimum 20. In the case of the edge sizing and the global growth rate, the differences in the results of the tangential forces are not significant. Due to limited space, the results of the aerodynamic loads for other grid parameters have not been presented in this article. Table 1 presents the mesh parameters assumed for all simulations presented here. The number of mesh elements for the two-bladed rotor is 104 924.
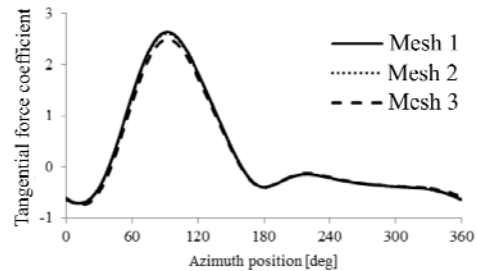

Fig. 6. Tangential force coefficient for three values of structured mesh growth rate.

Table 1 Mesh parameters.

Parameter of mesh	Value
First layer thickness [m]	6e-6
Number of layers of structured mesh	20
Growth rate of inflation mesh	1.2
Global growth rate	1.06
Edge sizing [m]	516.527

5.4   Simulation Parameters

The two-bladed rotor is computed for the tip speed ratio of 5.0, which corresponds to the water velocity at the inlet of 0.091 m/s and a constant angular velocity of 0.75 rad/sec. For slow moving water the turbulence intensity is almost equal to zero. In this paper the turbulence intensity is set to be 0.1% for all simulations presented here.

Simulations were performed utilizing the pressure-based solver with the SIMPLE algorithm for pressure-velocity coupling. Second order discretization schemes were employed for the governing flow equations. For gradient spatial discretization the least squares cell based method was selected.

In this paper transient solver was utilized. Unsteady simulations require a small time step size. Bangga et al. (2017) investigated three values of time step sizes that correspond to the rotor rotation angles of 1°, 0.5° and 0.25° for a small two-bladed vertical-axis wind turbine operating under dynamic stall conditions. The results obtained by Bangga at al. (2017) for the angles of 0.5 and 0.25 are similar. In the present investigations the time step size was equivalent to the rotor rotation angle 0.1°. The maximum number of iterations per each time step was established to be 20. The convergence was satisfied when the residuals were below 1e-06 in every time step.

In this paper the enhanced wall treatment method was used for the k-ε family models. In this near-wall modeling method the near-wall grid should be fine enough in order to compute the laminar sublayer (typically y+~1).

6. RESULTS AND DISCUSSION

6.1 Aerodynamic Blade Loads

The results of aerodynamic loads, the normal and the tangential force coefficients are presented in Figs. 7 and 8. The numerical results are compared with the experimental results of Strickland *et al.* (1981) and analytical results of Scheurich *et al.* (2011). The analytical results of Scheurich *et al.* (2011) are obtained using the Brown's Vorticity Transport Model (VTM) and the experimental airfoil characteristics of NACA 0012. The normal and tangential loads taken from Scheurich *et al.* (2011) are performed for the section at the mid-span of the long blade of the Darrieus-type wind turbine.

The CFD results of the authors are performed for four turbulence models: the SST k-ω, the k-ε, the RNG k-ε and the Realizable k-ε. Analyzing the obtained CFD results of the tangential loads as well as the results of Scheurich *et al.* (2011), it can be seen from Fig. 7. that the character of all computed loads is very similar, especially for the upwind part of the rotor. The maximum value of the tangential force coefficient from the experiment of Strickland *et al.* (1981) for the upwind part of the rotor, of about 3.6, is not reached by CFD and by the VTM approach. For the family turbulence models k-ε, the results of the tangential loads are identical. In the case of the SST k-ω turbulence model, the tangential loads are slightly different for upwind part of the rotor in comparison with the k-ε models and much better in comparison with the experimental results for the downwind part of the rotor. CFD methods and the Brown's Vorticity Transport Model have not predicted the second peak of the tangential loads at azimuth of about 260deg. The results of the normal loads are very similar for all numerical and analytical approaches (Fig. 8). Some differences in numerical and experimental results are seen for the azimuth in the range between 200deg and 350deg.
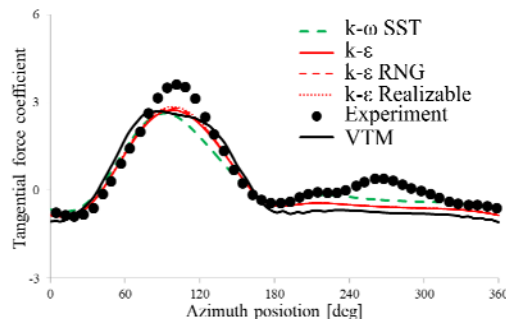

Fig. 7. Tangential loads vs. azimuth position. The comparison between CFD, the experimental data (Strickland *et al.* (1981)) and the Brown's Vorticity Transport Model (Scheurich *et al.* (2011)).
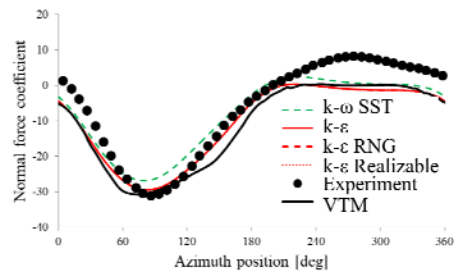

Fig. 8. Normal loads vs. azimuth position. The comparison between CFD, the experimental data (Strickland *et al.* (1981)) and the Brown's Vorticity Transport Model (Scheurich *et al.* (2011)).

Scheurich *et al.* (2011) concluded that the sudden change in aerodynamic loads at the downwind part of the rotor is caused by the interaction between the blades and the aerodynamic wake for the three-dimensional rotor. In other words, the change in the aerodynamic loads is caused by the 3D effects, although the intention of Strickland *et al.* (1979a) was taking measurements of aerodynamic blade loads for the conditions corresponding to the two-dimensional flow. These effects led to local dynamic stall near the tips of the blades, therefore simplified aerodynamic models for the Darrieus-type wind turbines should take into account a dynamic stall model.

The cause of the hump in the tangential force coefficient seen in the downwind part of the rotor at the azimuth in the range between 260° and 280° (Fig. 7) could also be caused by the blade passing the wake and the vortex structure from the second blade. Rogowski *at al.* (2016) presented 2.5D unsteady CFD analysis of a single one-bladed wind turbine operating at a tip speed ratio of 5 employing the scale adaptive simulation (SAS) approach. The SAS turbulence model allows the resolution of the turbulent spectrum in unstable flow conditions. Unsteadiness occurs at upwind part of the rotor and it is convected downstream with the flow. The analysis confirmed the wake-blade interaction between the rotor blade and its own aerodynamic wake in the downwind part of the rotor. The flow past a two-bladed rotor is even more complex. Therefore, the choice of classic two-equation turbulence models may be insufficient to study all physical phenomena arising in the flow. The use of large eddy simulation LES models seems to be justified. However, CFD analysis applying the LES approach is very expensive.

According to Strickland *et al.* (1981) the visible hump on the experimental curve of the tangential loads at the azimuth of 270deg can be caused by misalignment errors in the blade mounting. Strickland wrote: "Errors on the order of 1° in the blade angle of attack could cause this level of deviation from the analysis". Therefore, the authors of the paper have performed CFD computations of the same 2D two-bladed rotor with various mounting errors. Two constant displacements forwards and backwards of blades with a length of *b*=2mm and two constant pitch angles *γ* of -1° and +1° are assumed, Fig. 9.
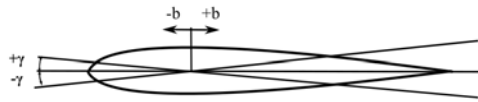
Fig. 9. Test cases for the various settings of the blade.

Results of the tangential and the normal force coefficients for two displacements and for two pitch angles are presented in Figs. 10 and 11, respectively. The computations are made using the RNG k-ε turbulence model. The obtained aerodynamic blade loads have been compared with the reference results (black solid line) for no pitch and no displacement (*b*=0 and *γ*=0). The final results are also compared with the experimental data. The results clearly show that for the blades moved backwards as well as a negative toe angle, the results of the tangential force coefficients are higher than reference values for the upwind part of the rotor. For the blades moved forward and for a positive toe angle, the tangential force behaves as in the case of the reference for the windward side of the rotor. The best results for the downwind part of the rotor can be observed for the positive toe angle of the blades. The results of the normal force coefficient are similar for all cases. This simple observation can indicate that the blades deflect during rotation due to water pressure. Even for the ideal case of the blade assembly, the one end support of the blades can lead to significant displacements.
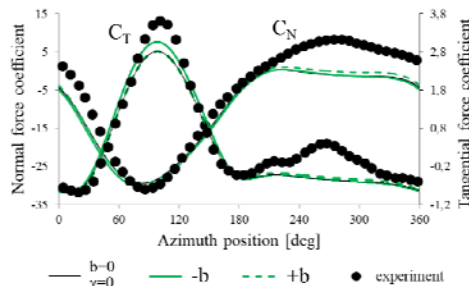

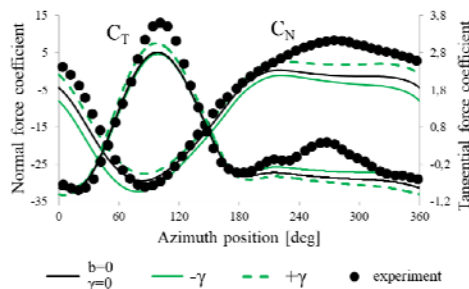**Fig. 10. Normal and tangential force coefficients for various settings of the blade.**

Fig. 11. Normal and tangential force coefficients for various settings of the blades.

6.2 Static Pressure and Velocity Magnitude

The authors of this paper have performed the analysis of pressure and velocity distribution around the rotor airfoil. The contours of the static pressure

for one blade of the rotor are given in Fig. 12. The contours are presented at six azimuthal positions every 60°. The results are computed using the SST k-ω turbulence model. At the azimuthal position of 0°, the pressure distribution is not symmetrical. This explains the non-zero value of tangential force (see Fig. 7). The largest pressure difference is visible in the upwind part of the rotor. In this half-cycle of the rotor a large area of negative pressure is observed on the inner surface of the airfoil.
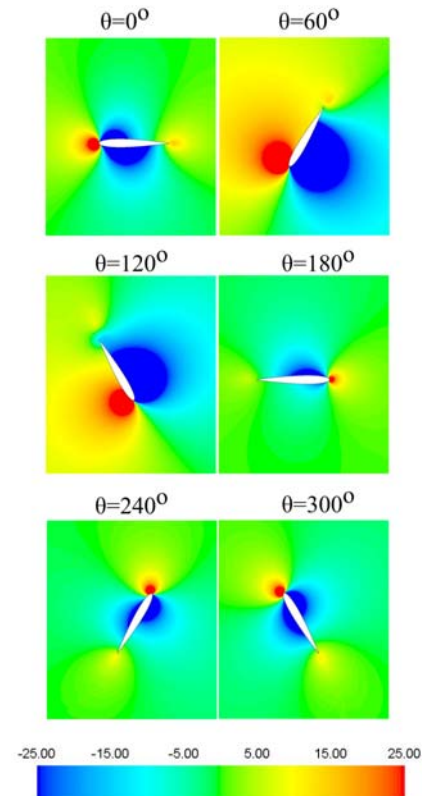

Fig. 12. Contours of instantaneous static pressure at six azimuthal positions.

The instantaneous contours of velocity magnitude at the same azimuth angles are also presented, Fig. 13. The results show two regions of high velocity magnitude near the leading and trailing edges of the airfoil. At the azimuthal position of 120° the regions of the velocity magnitude are the largest. This indicates flow separation taking place on the inner surface of the airfoil.

6.3 Wake Velocity Profiles

Nowadays the wake behind the rotor has become very important issue because turbines are mostly erected in wind farms. Velocity field is estimated quantitatively and qualitatively in this paper. The by computing velocity profiles behind the rotor. Two velocity components, given as streamwise and lateral perturbation velocities are computed using CFD at one rotor diameter downstream from the rotor center and compared with the experiment of Strickland *et al.* (1981). The second qualitatively estimation has been carried out by using streak lines first quantitatively estimation have been performed in CFD computations based on the experiment by
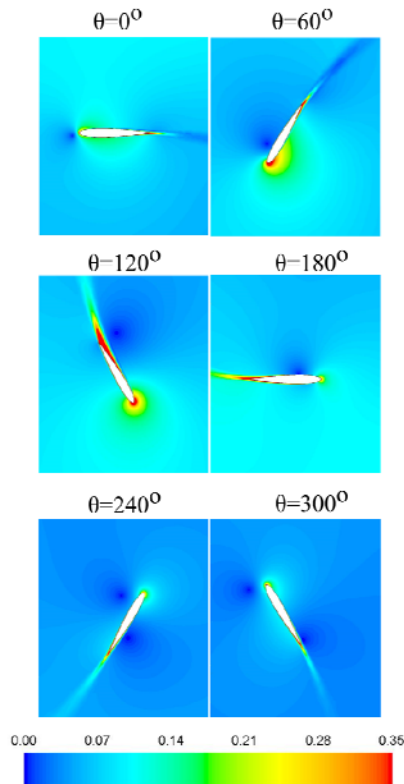
Fig. 13. Contours of instantaneous velocity magnitude at six azimuthal positions.

Strickland *et al.*, (1979b). The purpose of this test is to show how trajectories of shed vortices follow one of the rotor blades. Streak lines in the experiment were made using dye injected through the trailing edge of the airfoil. Visualization of streak lines by CFD has been made using the discrete phase model (DPM) with the unsteady particle tracking. The DPM model was simplified by choosing a massless particle type of injected substance. Massless particles were injected through the trailing edge of the airfoil and convected in the unsteady wake flow.

Figure 14 presents the streamwise, V_x, and lateral, V_y, perturbation velocities computed using the RNG k-ε turbulence model for the two-bladed rotor configuration based on the Strickland's *et al.* (1981) experiment. The streamwise and the lateral perturbation velocities are expressed in dimensionless form as: $u=V_x/V$ and $v=V_y/V$, respectively. Blue dots in the Fig. 14 present the experimental results of streamwise perturbation velocities whereas the numerical equivalent of streamwise perturbation velocities is shown using black dotted lines. Lateral perturbation velocities are presented using red triangles in the case of experimental results and dashed lines for numerical predictions. Looking at the resulting velocity profiles in Fig. 14 one can observe that that the results obtained by CFD correspond to the experiment very well in the range of the *y/R* ratio between -1 and 1. With the increase in the *y/R* ratio the, deviation of the results of the *u* and *v* velocity components is visible in comparison to the experimental results. The reason for this behavior is most likely 3D effects. In fact, the wind turbine is

three-dimensional and the fluid flow past the rotor is more complex. Scheurich *at al.* (2011) presented that for the three-dimensional straight bladed rotor the trailing vortices appear at the blade tips and move downstream of the rotor. A tip vortex trailed by the blade located in the upwind part of the rotor interacts with the second blade located in the downwind part of the rotor changing locally the angle of attack. This can be the direct cause of the velocity difference for *y/R> 1*. Another reason may be an insufficient number of mesh cells in the rotor wake.
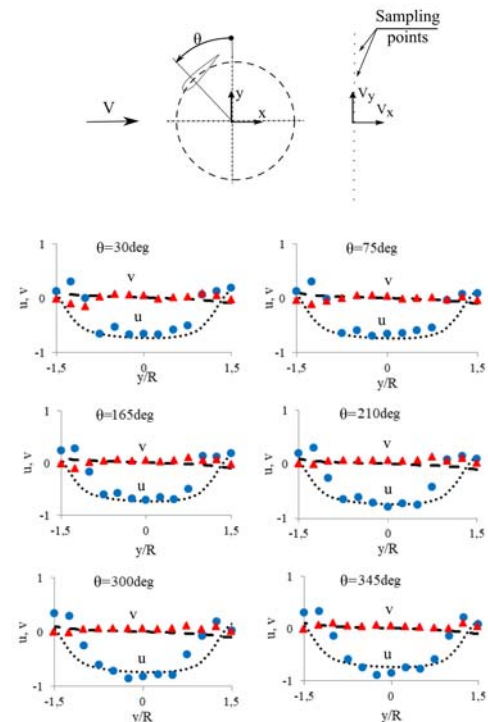

Fig. 14. Velocity profiles at six azimuth positions. Velocities are expressed in dimensionless form as: $u=V_x/V$ and $v=V_y/V$.

The results of the aerodynamic wake profiles may also significantly depend on the choice of the turbulence model. In this investigation only the SST k-ω turbulence model and the k-ε family model were used for analysis. Fig. 15 presents the comparison of wake velocity profiles at the azimuth angle of 30° computed using the SST k-ω turbulence model and the k-ε family models. The results of *u* and *v* velocity components are almost the same for all examined turbulence models.

Numerical and experimental results of streak lines for the two-bladed rotor operating at a tip speed ratio of 5 are presented in Fig. 16. Because of diffusion of dye only the first two or three revolutions of the dye particles are visible in the pictures. However, again a good agreement between computed and experimental results are observed.

6.4   Airfoil Characteristics

This section presents numerical analysis on the performance of NACA 0012 airfoil. CFD investigations have been performed using the same grid as for the unsteady case displayed in Fig. 5.
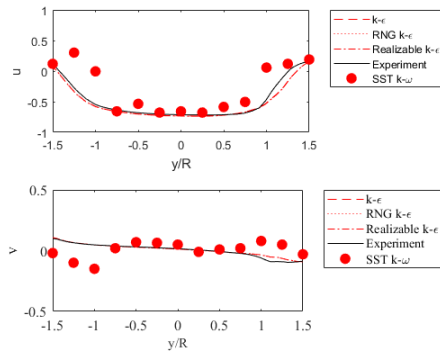
Fig. 15. Velocity profiles at the azimuth position of 30° for four turbulence models.
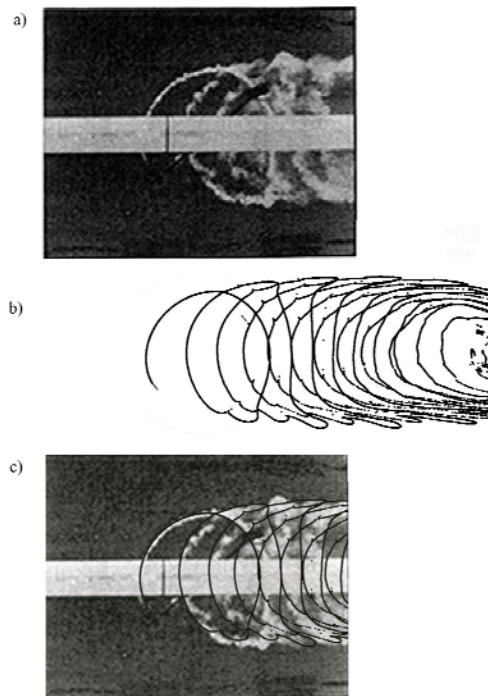

Fig. 16. Streak lines for: (a) experiment (Strickland *et al.* (1979b)), (b) CFD, (c) experiment and CFD.

The non-dimensional lift and drag coefficients, C_L and C_D, are obtained using the same turbulence models: the standard k-ε; the RNG k-ε; the Realizable k-ε and the SST k-ω. Numerical investigations are performed for the Reynolds number corresponding to the blade Reynold number of the moving blade. The Reynolds number is defined as: $Re=Vc\rho/\mu$, where c is the chord length, ρ is the water density and μ is the dynamic viscosity of the fluid. In this investigation the Reynolds number taken, for steady-state analysis is 40 000. The obtained steady state results of the lift and drag coefficients are compared with the experiment presented by Paraschivoiu (2002). The lift and drag coefficients as functions of angle of attack are given in Figs. 17 and 18. The computed characteristics of the lift coefficient are agree with the experiment up to the critical angle of attack. In the experiment, the critical angle of attack is measured to be 6°, this value is not predicted by CFD. The results of the drag coefficient obtained by k-ε turbulence models

are slightly overestimated in comparison with the experiment. The SST k-ω model better covered the experimental results of the drag coefficients.

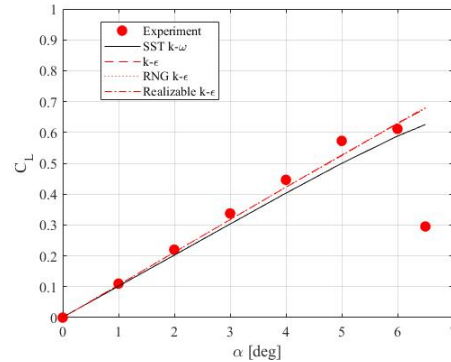**Fig. 17. Lift coefficient vs. angle of attack, Re=40,000.**
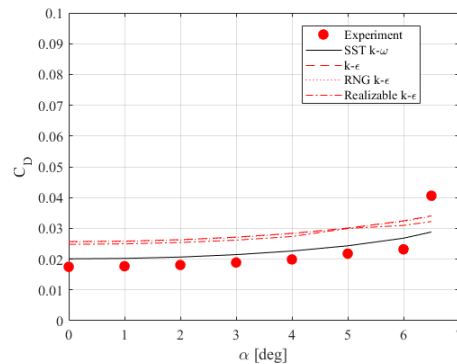

Fig. 18. Drag coefficient vs. angle of attack, Re=40,000.

5. CONCLUSION

The most important purpose of this work was the comparison of aerodynamic blade loads and wake velocity profiles computed by CFD with the experiments for the vertical axis wind turbine. The intention of the authors was also to investigate the effects of mesh topology on numerical solution, examination of effects, estimation of aerodynamic blade loads in terms of blade assembly and the selection of the major turbulence model/models.

The hybrid mesh consisting of structured quadrilateral elements near airfoils and unstructured mesh consisting of triangular elements elsewhere is suitable for unsteady simulation of vertical axis wind turbines with the Darrieus-type rotor.

The CFD results of aerodynamic loads are comparable with the experimental one. All used turbulence models give satisfactory results, however, peaks of the tangential load both for the upwind and the downwind parts of the rotor are not achieved by CFD and the VTM. The results of the normal load are satisfactory for all test cases, however, almost all CFD and VTM results are slightly lower in comparison to experimental ones for the azimuth range between 220 and 360 deg.

The accuracy of the blade mounting is a very important factor in determining the aerodynamic

forces experimentally. The displacement of the blade of 2 millimeters or the change of constant pitch angle of 1 degree may significantly change the characteristics of the tangential load.

The CFD results of wake structure (velocity profiles and streak lines) are very reasonable compared with the experiments.

The SST k-ω turbulence model better predicts drag coefficients for angles of attack up to the critical angle of attack in comparison with the k-ε family models. Both the SST k-ω turbulence model and the k-ε family models gives satisfactory results of lift coefficients in the linear part of the characteristic.

REFERENCES

Allet, A., S. Hallé and I. Paraschivoiu (1999). Numerical Simulations of Dynamic Stall Around an Airfoil in Darrieus Motion. *Journal of Solar Energy Engineering* 121(1), 69-76.

Amet, M., T. Maître, C. Pellone and J. L. Achard (2009). 2D Numerical Simulations of Blade-Vortex Interaction in a Darrieus Turbine. *Journal of Fluids Engineering* 131(11), 111103-111103-15.

Bangga, G., Hutomo, G., Wiranegara R. and H. Sasongko (2017). Numerical study on a single bladed vertical axis wind turbine under dynamic stall. *Journal of Mechanical Science and Technology* 31(1), 261-267.

Bianchini, A., Balduzzi, F., Ferrara, G. and L. Ferrari (2016). *Energy Conversion and Management* 111, 329–338

Ferziger, J. H. and M. Perić (2002). *Computational Methods for Fluid Dynamics*. Springer-Verlag, Berlin, Germany.

Hansen, M. O. L. and D. N. Sørensen (2001). CFD Model for Vertical Axis Wind Turbine. *Proceedings of the European Wind Energy Conference*, Copenhagen, 485-488.

Laneville, A. and P. Vittecoq (1986). Dynamic stall: The case of the vertical axis wind turbine. *Journal of Solar Energy Engineering* 108(2), 140-145.

Oler, J. W., J. H. Strictland, B. J., Im and G. H. Graham (1983). Dynamic Stall Regulation of the Darrieus Turbine. *Sandia National Laboratories, Technical Report*, SAND83-7029.

Paraschivoiu, I. (2002). *Wind Turbine Design: With Emphasis on Darrieus Concept*. Presses Internationales Polytechnique, Quebec, Canada.

Ponta, F. L. and P. M. Jacovkis (2001). A vortex model for Darrieus turbine using finite element techniques. *Renewable Energy* 24, 1-18.

Qamar S. B. and I. Janajreh (2017). A comprehensive analysis of solidity for cambered Darrieus VAWTs. *International Journal of Hydrogen Energy* 42(30), 19420-19431.

Rajagopalan, R. G. and J. B. Fanucci, (1985). Finite difference model for vertical axis wind turbines. *Journal of Propulsion and Power* 1(6), 432-436.

Rezaeiha A., Kalkman I. and B. Blocken (2017). CFD simulation of a vertical axis wind turbine operating at moderate tip speed ratio: Guidelines for minimum domain size and azimuthal increment. *Renewable Energy* 107.

Rogowski, K. (2014). *Analysis of Performance of the Darrieus Wind Turbines*. Ph.D. Thesis, Warsaw University of Technology, Warsaw, Poland.

Rogowski, K., Hansen, M. O. L., Maroński, R. and P. Lichota (2016). Scale Adaptive Simulation Model for the Darrieus Wind Turbine. *Journal of Physics: Conference Series* 753 022050.

Rogowski, K., R. Maroński and J. Piechna (2017). Numerical Analysis of a Small-Size Vertical-Axis Wind Turbine Performance and Averaged Flow Parameters Around the Rotor. *Archive of Mechanical Engineering* 64 (2), 205-218.

Scheurich, F., T. M. Fletcher and R. E. Brown (2011). Simulating the aerodynamic performance and wake dynamics of a vertical-axis wind turbine. *Wind Energy* 14, 159–177.

Shamsoddin, S. and F. Porté-Agel (2014). Large Eddy Simulation of Vertical Axis Wind Turbine Wakes. *Energies* 7, 890-912.

Shen, W. Z., J. N. Sørensen and J. H. Zhang (2009). The Actuator Surface Model: A New Navier-Stokes Based Model for Rotor Computations. *Journal of Solar Energy Engineering* 131(1), 011002-011002-9.

Simão Ferreira, C. J., H. Bijl, G. J. W. Bussel and G. A. M. Kuik, (2007). Simulating Dynamic Stall in a 2D VAWT: Modeling strategy, verification and validation with Particle Image Velocimetry data. *Journal of Physics: Conference Series* 75.

Simão Ferreira, C. J., G. J. W. Bussel, G. A. M. Kuik and F. Scarano (2011). On the Use of Velocity Data for Load Estimation of a VAWT in Dynamic Stall. ASME. *Journal of Solar Energy Engineering* 133(1), 011006-011006-8.

Strickland, J. H., B. T. Webster and T. Nguyen (1979a). A Vortex Model of the Darrieus Turbine: An Analytical and Experimental Study. *Sandia National Laboratories, Technical Report*, SAND79-7058.

Strickland, J. H., B. T. Webster, and T. Nguyen, (1979b). A Vortex Model of the Darrieus Turbine: An Analytical and Experimental Study. *Journal of Fluid Engineering* 101(4), 500–505.

Strickland, J. H., T. Smith and K. Sun (1981). A Vortex Model of the Darrieus Turbine: An

Analytical and Experimental Study. *Sandia National Laboratories, Technical Report*, SAND81-7017.

Velasco, D., Lopez Mejia O. and S. Laín (2017). Numerical simulations of active flow control with synthetic jets in a Darrieus turbine. *Renewable Energy* 113, 129-140.

Wang, Y., Sun, X. J. Zhu, B. Zhang, H. J. and D. G. Huang (2016). Effect of blade vortex interaction on performance of Darrieus-type. *Renewable Energy* 86, 316-323

Wickens, R. H. (1985). Wind Tunnel investigation of Dynamic Stall of an NACA0018 Airfoil Oscillating in Pitch. *NRC Aeronautical Note*, NAE-AN-27.